

Supporting Information for:
**Electron-Transparent Thermoelectric Coolers Demonstrated with
Nanoparticle and Condensation Thermometry**

William A. Hubbard,^{1,2,†} Matthew Mecklenburg,^{3,†} Jared J. Lodico,^{1,2,†} Yueyun Chen,^{1,2} Xin
Yi Ling,^{1,2} Roshni Patil,^{1,2} W. Andrew Kessel,^{1,2} Graydon J. K. Flatt,^{1,2} Ho Leung Chan,^{1,2}
Bozo Vareskic,^{1,2} Gurleen Bal,^{1,2} Brian Zutter,^{1,2} and B. C. Regan^{1,2,*}

¹*Department of Physics & Astronomy and California NanoSystems Institute, University of
California, Los Angeles, California 90095 USA.*

²*California NanoSystems Institute, University of California, Los Angeles, California 90095 USA.*

³*Core Center of Excellence in Nano Imaging, University of Southern California, Los Angeles,
California, 90089, U.S.A.*

†These authors contributed equally

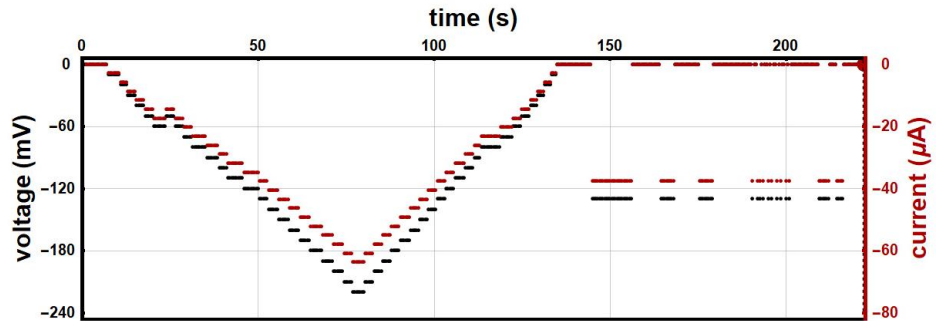
*Corresponding author: regan@physics.ucla.edu

Thermoelectric Cooling: Condensation Thermometry



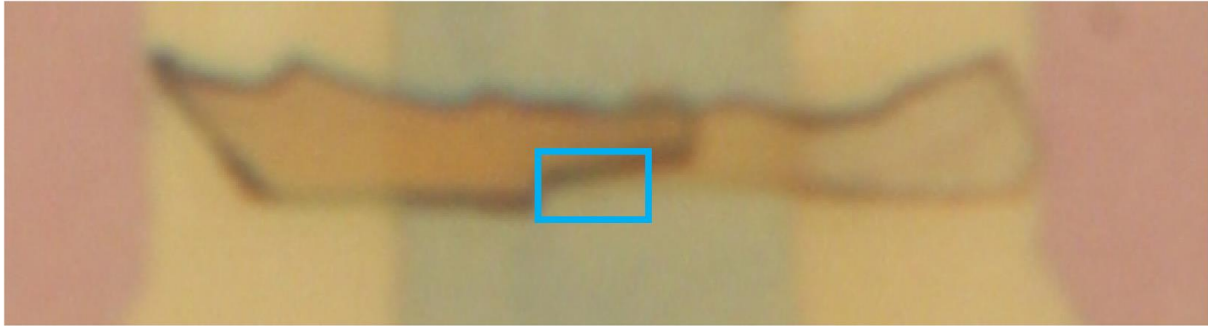
3 μm

UCLA Regan Group



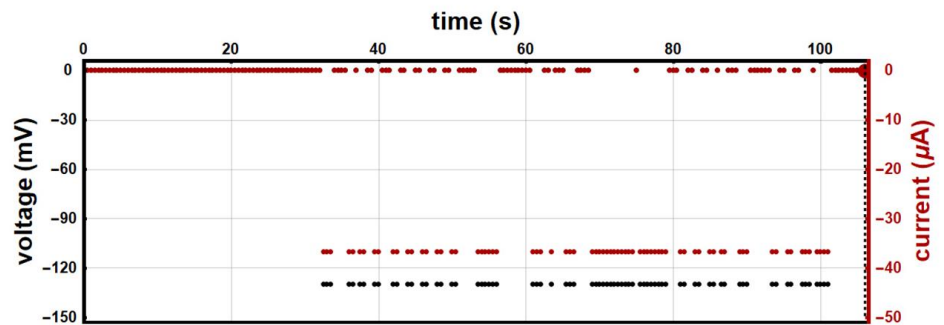
Supporting Movie 1: This image is the last frame from an optical movie of a TEC device condensing a dew drop near the heterojunction. The humidity and temperature of the room are 52% and 22.1 $^{\circ}\text{C}$ respectively, which corresponds to a dew point of 11.8 $^{\circ}\text{C}$. The TEC device is mounted on a bulk Peltier module held at 15.7 $^{\circ}\text{C}$. During the voltage ramp from 0 to -220 mV a droplet forms, reaches a maximum size, and then nearly disappears. This growth process is then reversed as the voltage ramps back to 0 mV. Voltage pulses to -130 mV cause droplets to quickly form and disappear. See Figure 3 of the main text for further discussion.

Thermoelectric Cooling: Condensation Thermometry

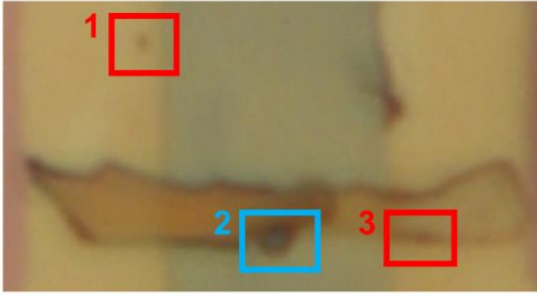


3 μm

UCLA Regan Group

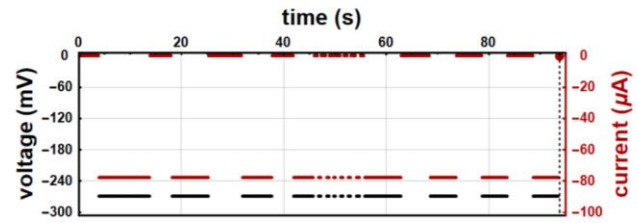


Supporting Movie 2: This image is the last frame from an optical movie of a TEC device condensing a small, but still subtly visible, droplet near the heterojunction. The humidity and temperature of the room are 52% and 22.2 °C respectively, which corresponds to a dew point of 11.9 °C. The TEC device is mounted on a bulk Peltier module held at 18.6 °C. Pulses of -130 mV cause a very small droplet to form and disappear, indicating a maximum cooling of $\Delta T_{\text{cool}} = -6.7$ K or better. The blue box highlights the region where the small droplet appears. See Figure 3 of the main text for further discussion.



5 μm

Thermoelectric Cooling: Condensation Thermometry

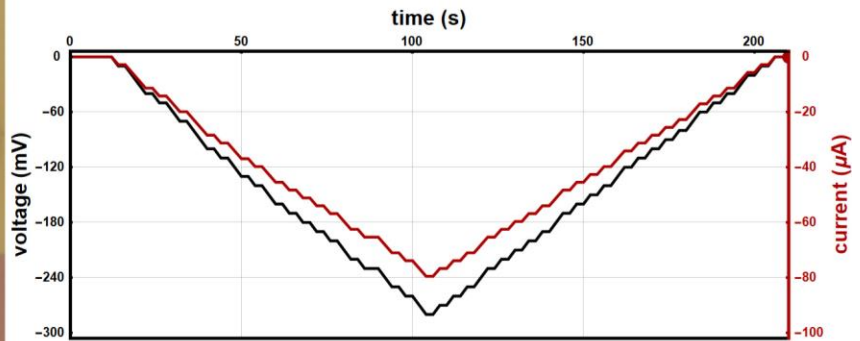


UCLA Regan Group

Supporting Movie 3: This image is the last frame from an optical movie of a TEC device demonstrating simultaneous heating and cooling in different regions while under bias. The humidity and temperature of the room are 51% and 22.1 °C respectively, which corresponds to a dew point of 11.5 °C. The TEC device is mounted on a bulk Peltier module held at 10.5 °C (*i.e.* 1.0 °C below the dew point). Droplets formed by the bulk module are highlighted by the red boxes 1 and 3. A voltage of -270 mV causes a dew drop to condense at the heterojunction highlighted by the blue box 2, and causes the droplets in boxes 1 and 3 to disappear. Over many cycles the formation of the droplet in box 2 is out of phase with the formation of droplets in boxes 1 and 3. See Figure 3 of the main text for further discussion.



Thermoelectric Cooling: Condensation Thermometry

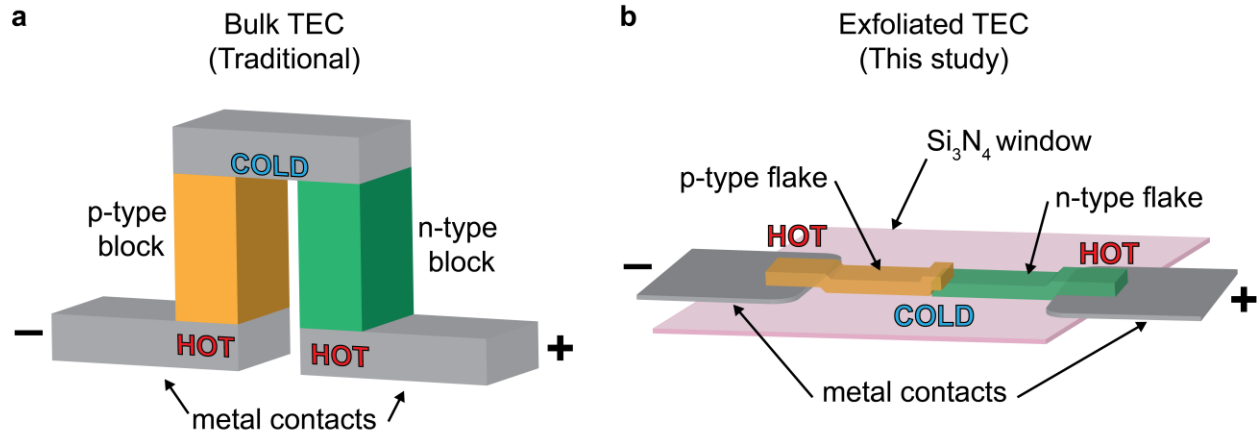


15 μm

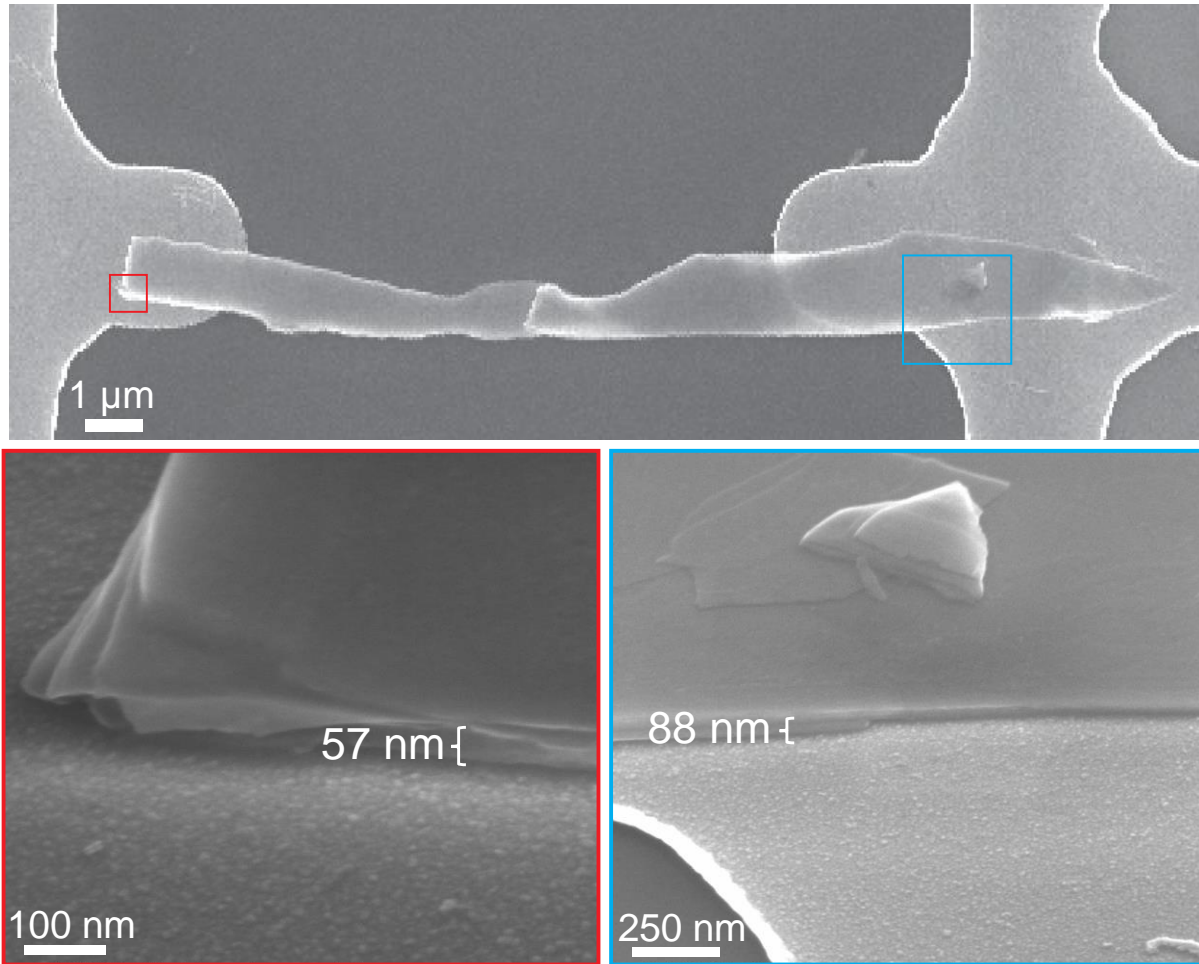
UCLA Regan Group

Supporting Movie 4: This image is the last frame from an optical movie of a TEC device condensing a large dew drop over the heterojunction. The humidity and temperature of the room are 51% and 22.1 °C respectively, which corresponds to a dew point of 11.5 °C. The TEC device is mounted on a bulk Peltier module held at 10.5 °C (*i.e.* 1.0 °C below the dew point). During a voltage ramp from 0 to -280 mV a large dew drop forms over the heterojunction. Other droplets are visible (~10 μm in diameter) away from the device and are a result of the chip temperature being lower than the dew point. Unlike Movies 1-3, which were collected using a Mitutoyo M Plan Apo 50× objective with an NA = 0.55, this movie was collected using a Mitutoyo M Plan Apo 10× objective with an NA = 0.28. See Figure 3 of the main text for further discussion.

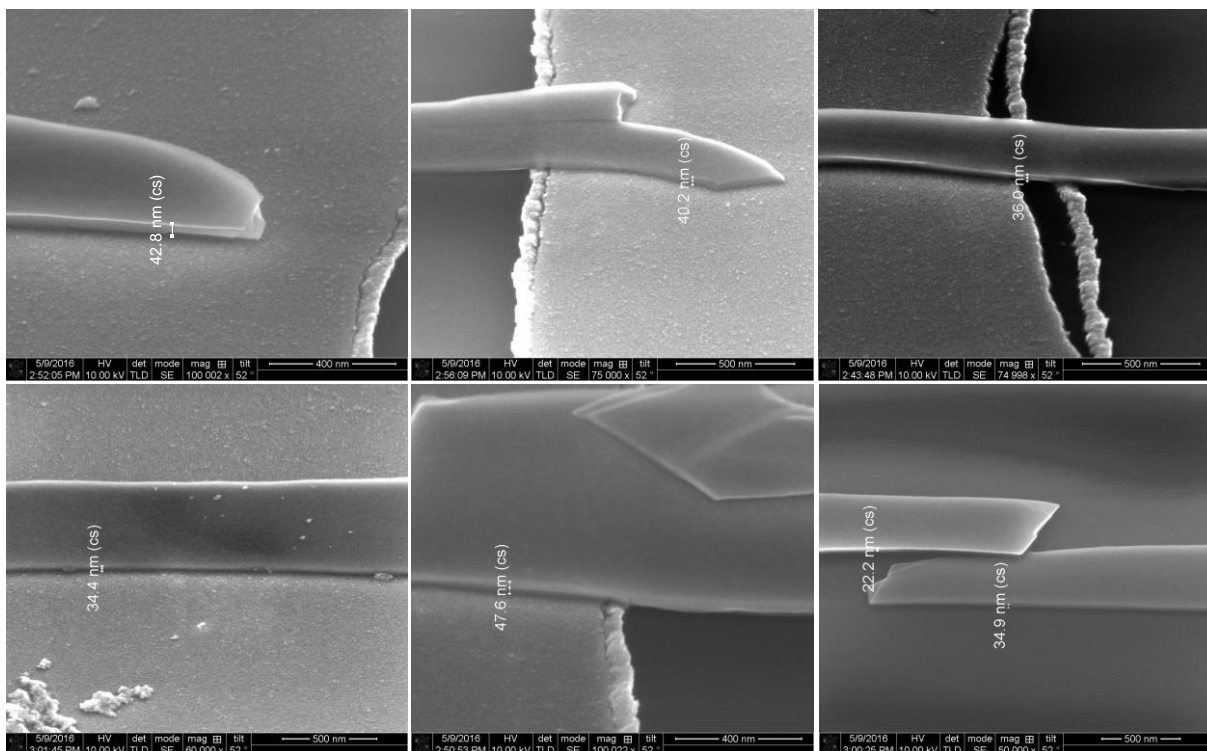
Supporting Figures



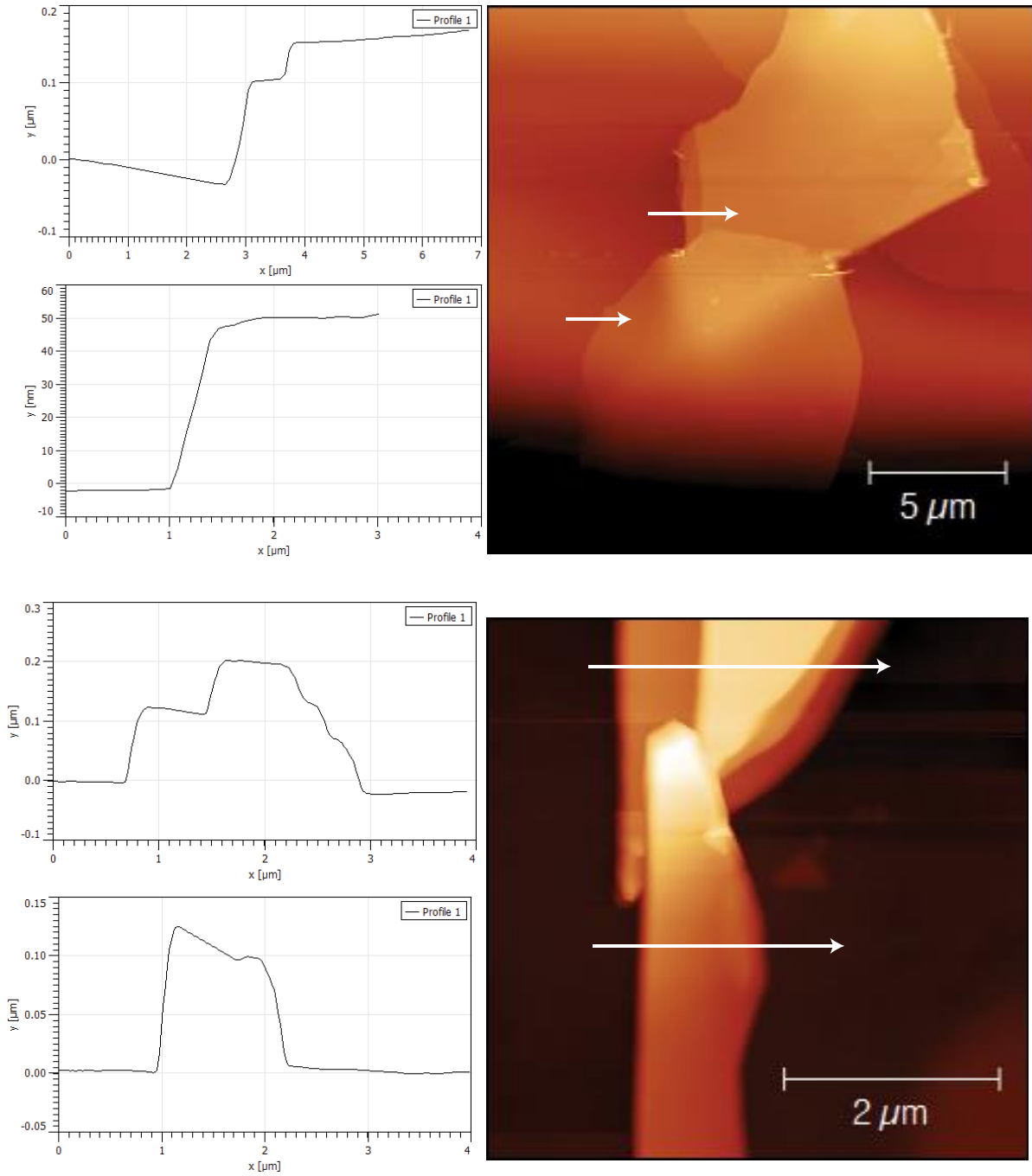
Supporting Figure 1: Thermoelectric device architectures. The traditional architecture (a) is referred to as 'II-type' because of its similarity with the shape of the Greek letter. 'T-type' and 'Y-type' geometries are also known. The architecture employed in this paper (b) uses very thin semiconducting flakes as opposed to the traditional blocks. It also does not have a metal connector between the semiconducting flakes, but makes the connection directly. When either of the (a-b) devices is employed as a TE cooler, the (standard) electrical current flows from positive to negative (right-to-left here), and the labeled regions heat or cool as indicated.



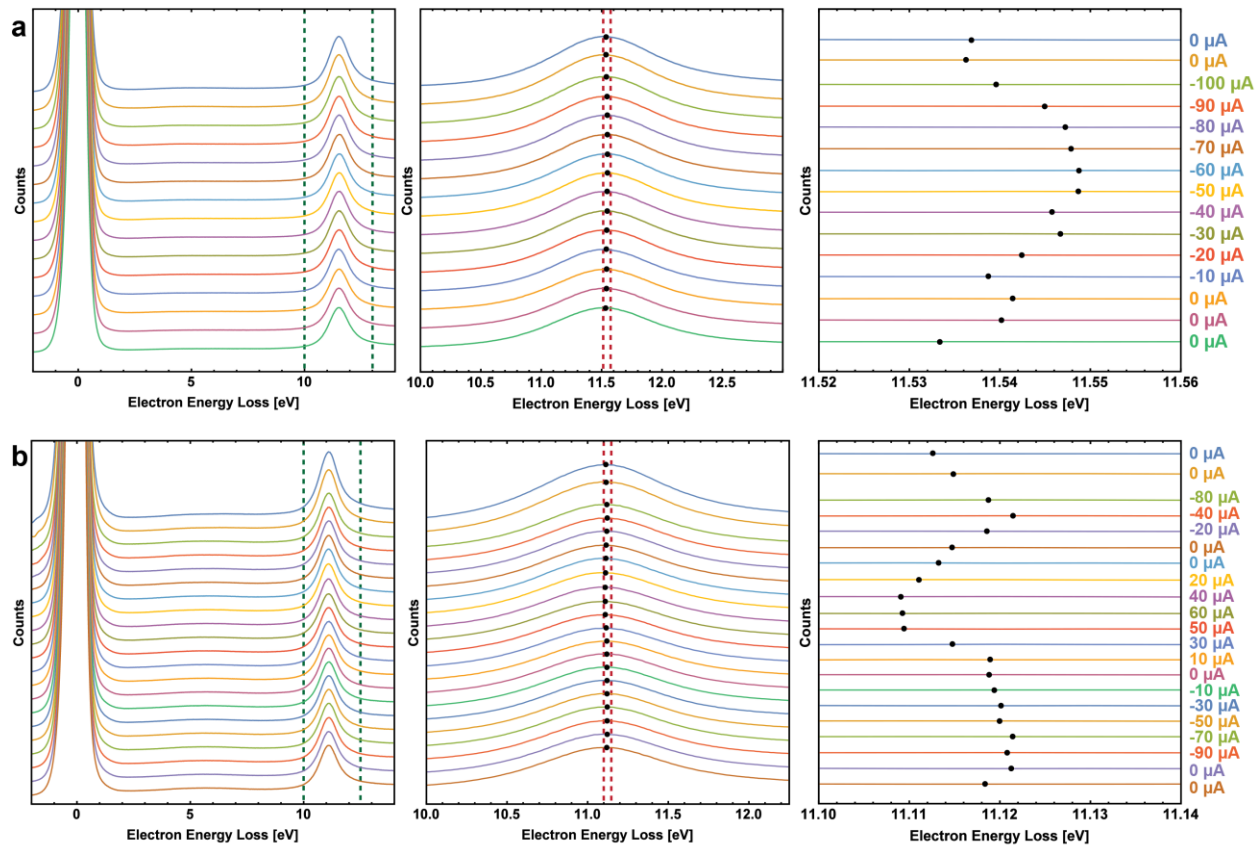
Supporting Figure 2: (top) SEM image of the TEC device from Figs. 1 and 2. (bottom) Higher magnification of the left and right flake/Pt interfaces acquired with a 52° sample tilt. The colored boxes in the upper image correspond to the areas shown at higher magnification in the two lower images. The indicated flake thickness measurements are corrected for the sample tilt. The left flake is approximately $8 \mu\text{m} \times 1 \mu\text{m} \times 0.06 \mu\text{m} = 0.5 \mu\text{m}^3$, and the right flake is approximately $11 \mu\text{m} \times 1.5 \mu\text{m} \times 0.09 \mu\text{m} = 1.5 \mu\text{m}^3$, for a total device volume of $2 \mu\text{m}^3$. The active device volume (between the Pt leads) is approximately $1 \mu\text{m}^3$. The thickness indicators are provided by the SEM software and are not more accurate than $\pm 10\%$.



Supporting Figure 3: SEM images showing thicknesses of flakes used to produce various TEC devices. All images were acquired with 52° sample tilt, with indicated thickness measurement tilt-corrected. The thicknesses shown are all in the range 22 – 48 nm. The thickness indicators are provided by the SEM software and are not more accurate than $\pm 10\%$.



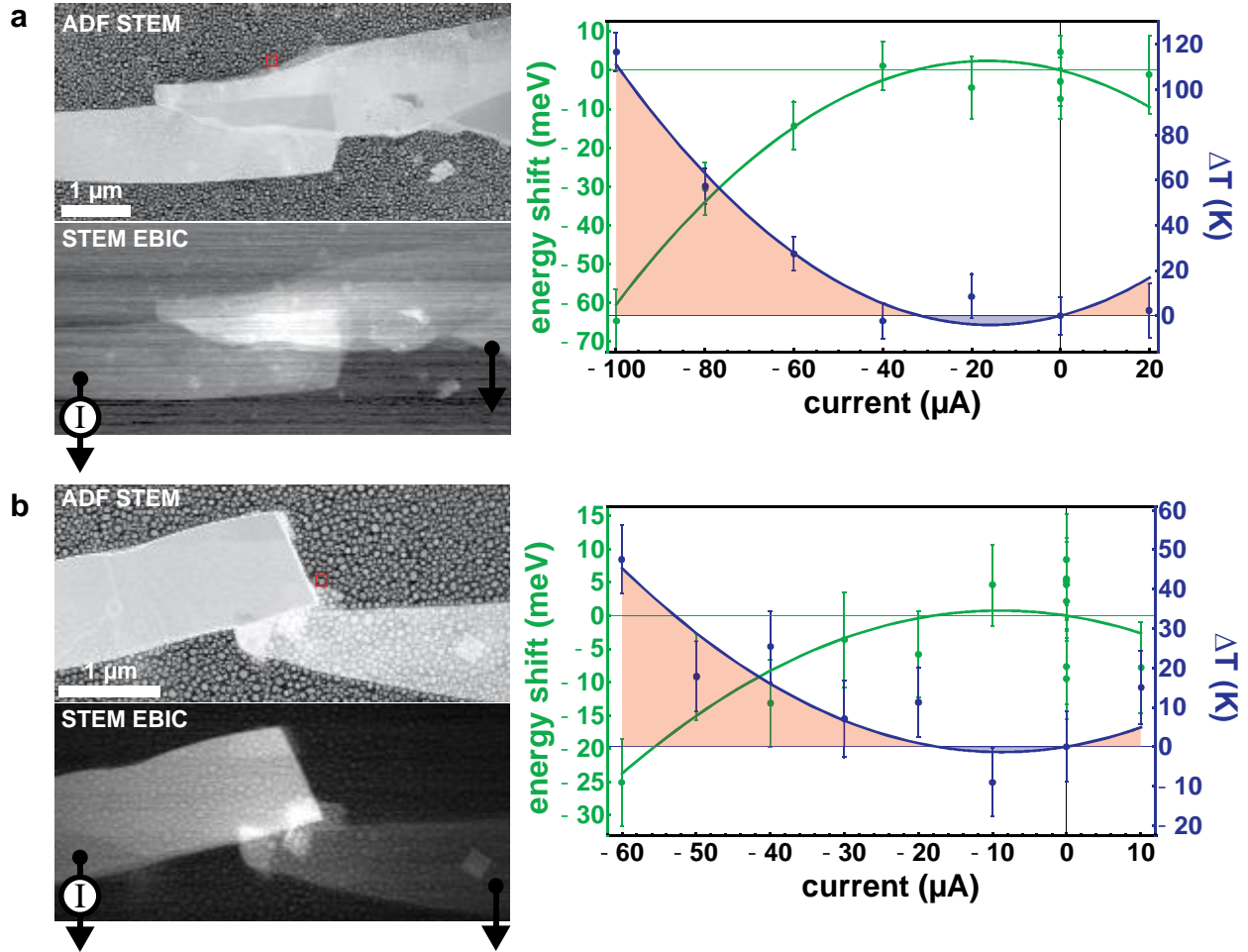
Supporting Figure 4: AFM data and line profiles showing thickness of each flake in two different TEC devices. The thicknesses shown range from 50 – 200 nm.



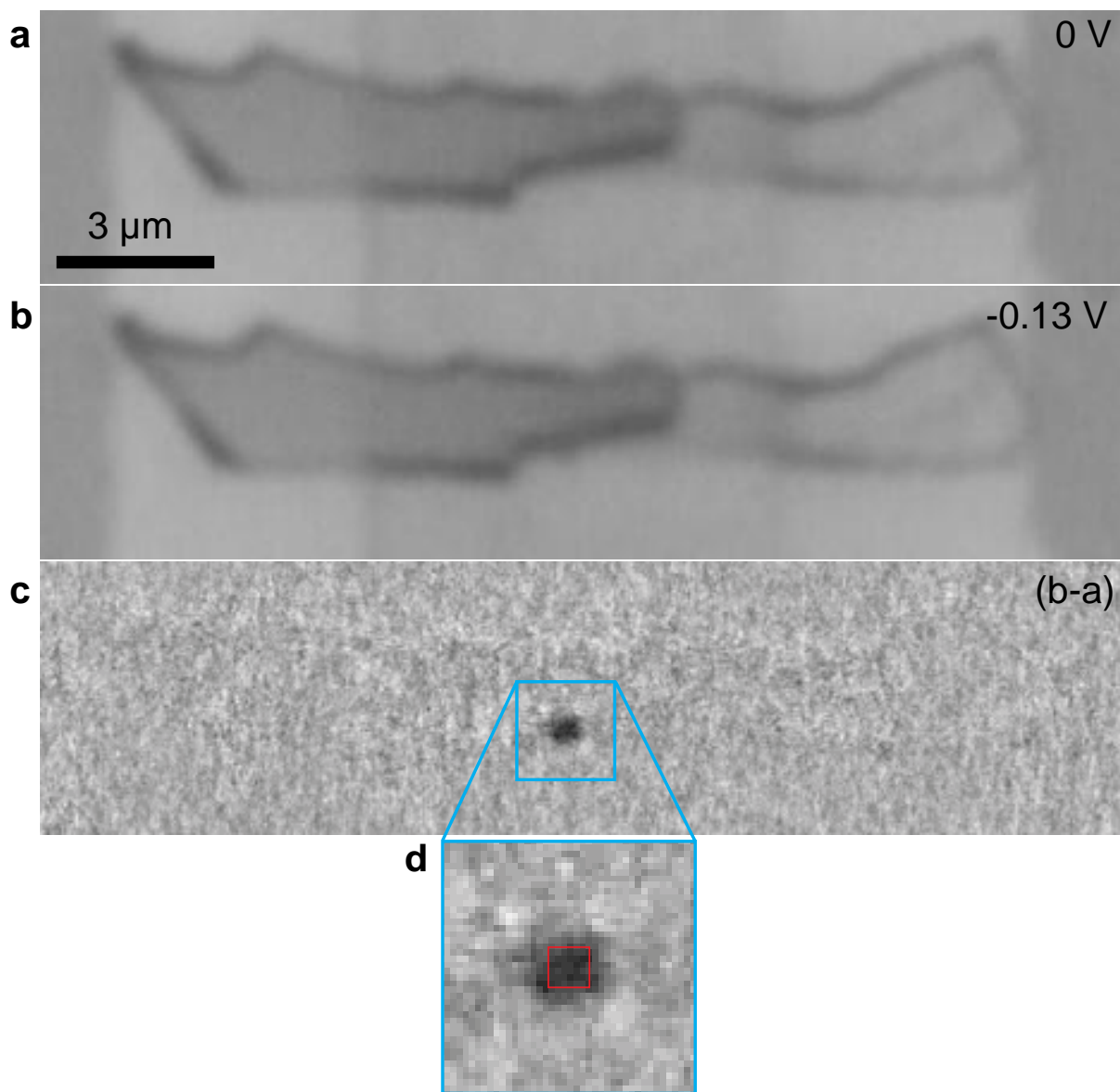
Supporting Figure 5: PEET data summary. (left column) Summed low-loss spectra from the EELS spectrum image in the indium nanoparticle used as a nanothermometer for the devices of Fig. 2 **(a)** and Fig. 3 **(b)**. (The green ROI in Fig. 2b, for example, shows the summed region on that particular indium nanoparticle.) In each plot the data are presented in the same sequence in which they were acquired, with the first data shown at the top. As is often the case with these devices, the Fig. 2 device changed as its bias was increased from zero the first time, so data from the initial ramp from zero to high bias are not shown. Color coordinated values (far right) show the TEC device current applied while each spectrum was acquired. The green dashed lines show the energy window displayed in the middle column. (middle column) Each plasmon peak is fit individually, and the center value of the fit is indicated with a black dot. The red, dashed lines show the energy window displayed in the right column. (right column) The energy shifts are shown in more detail. While the energy shifts are small compared to the plasmon energy, they are significant.

The analysis shown here differs from that in the main text. Here the spectra are summed and then fit, whereas for the main text the spectra are fit and then averaged. The latter method provides more detailed statistical information (which can be used to check for systematics), but the former method is presented here because it is simpler to explain graphically. The two approaches give results that are consistent to within the errors quoted.

Finally, the ~ 0.4 eV shift in the zero bias value of the In plasmon's energy between **(a)** and **(b)** is an artifact of a spectrometer recalibration, with **(b)** being probably more accurate.



Supporting Figure 6: ADF STEM and STEM EBIC images of two additional TEC devices. The small red boxes in the ADF STEM images indicate the nanoparticle on which PEET is performed. The data in (a) and (b) indicate that these devices have a ΔT_{cool} of -4 ± 10 K and -1 ± 8 K, respectively. Although little cooling occurs in these devices, the data are not symmetric about zero current, which indicates the presence of a (linear) cooling term in addition to the usual (quadratic) Joule-heating term.



Supporting Figure 7: Images showing the green color channel of two frames extracted from Supporting Movie 2 and a difference image. The two images show the TEC without (a) and with (b) the cooler energized. The difference image (c), showing b-a, highlights the tiny droplet that appears when the heterojunction is cool. A zoomed-in view (d) of the droplet in (c) is overlaid with a $300 \text{ nm} \times 300 \text{ nm}$ red box for size reference.

PEET curve fitting

Each spectrum image is a three-dimensional dataset consisting of an EELS spectrum for each pixel in two-dimensional real-space field-of-view. Extracting the spectra, one-by-one, from the circular spatial region centered on the nanoparticle, where the plasmon signal is strong (Fig. 2b, inset), we fit the zero-loss-peak (ZLP) and the first indium plasmon to determine the plasmon energy E_p , which is defined to be the difference between the peak centers. The fits are done pixel-by-pixel and not on the sum spectrum (Fig. 2b, plot) because the nanoparticle thickness varies, which leads to a varying background contribution from the silicon nitride plasmon.¹ After a rough spectrum alignment which places the spectrum maximum at 0 eV, the ZLP is fit to a Gaussian (three fit parameters: center, width, and amplitude) using a fit window of 0.48 eV centered on -0.03 eV. The indium plasmon is fit to a Lorentzian (four fit parameters: center, width, amplitude, and background amplitude) in a fit window of 1.15 eV centered on 11.56 eV. The background is due to the influence of the Si_3N_4 plasmon, modeled as a Lorentzian. The Si_3N_4 plasmon's Lorentzian center and width are determined separately by fitting a corner region of the same spectrum image, away from the indium nanoparticle. For the device in Fig. 2, after finding ≈ 700 values for the indium plasmon energy in a circular region of interest (30 pixel-diameter) centered on the nanoparticle, we calculate the weighted mean to arrive at the plasmon energy corresponding to that particular value of the TEC applied bias. The size of the ROI and thus the number of spectra contributing to the final plasmon energy value vary due to the varying dimensions of the imaged nanoparticles on each device.

We determine the plasmon energy at zero current by fitting all plasmon energies, which gives each point equal weight in determining the zero current value. This zero value is used to determine the energy shift for each data point. Except at zero current, where the central value is zero by construction and the error bar reflects the error in the fit, the plasmon energy shifts at each current are converted to temperatures using indium's coefficients of thermal expansion and the relation²:

$$\Delta T \equiv T - T_0 = \frac{\alpha_1}{2\alpha_2} \left(\sqrt{1 - \frac{8R\alpha_2}{3\alpha_1^2}} - 1 \right). \quad (1)$$

Here we take temperature to change the number density according to $n(T) \approx n(T_0)[1 - 3f(T)]$, where $f(T) \equiv \int_{T_0}^T \alpha(T')dT' \approx \alpha_1\Delta T + \alpha_2\Delta T^2$, and the α 's parametrize the linear (as opposed to volume) thermal expansion. Equation 1 thus gives ΔT as a function of the normalized change in the plasmon energy, $R \equiv (E(T) - E(T_0))/E(T_0)$. For indium, $\alpha_1 = 30.7 \times 10^{-6} \text{ K}^{-1}$, $\alpha_2 = 2.1 \times 10^{-8} \text{ K}^{-2}$ (Ref. 3). Linearizing Eq. 1 gives $\Delta T \approx -2\Delta E_p / (3E_p\alpha_1)$, indicating that +1 meV peak shift corresponds to a roughly -2 K temperature shift.

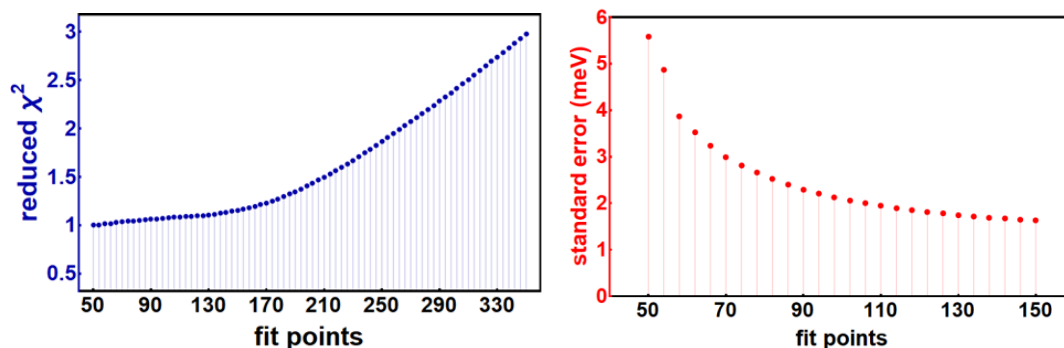
The minimum temperature value is computed through a weighted fit of the changes in temperature as a function of current. The error in the minimum current value has two contributions that we add linearly. The statistical error we determine by setting the reduced chi-squared statistic for each fit equal to unity (which effectively gives an error approximately equal to the error on each point divided by the square root of the number of points). The systematic error we take equal to the standard error in the mean of the changes in temperature implied by the zero-current plasmon energy measurements, which have a wider spread than expected based on purely statistical considerations.

Procedure for determining peak fitting windows

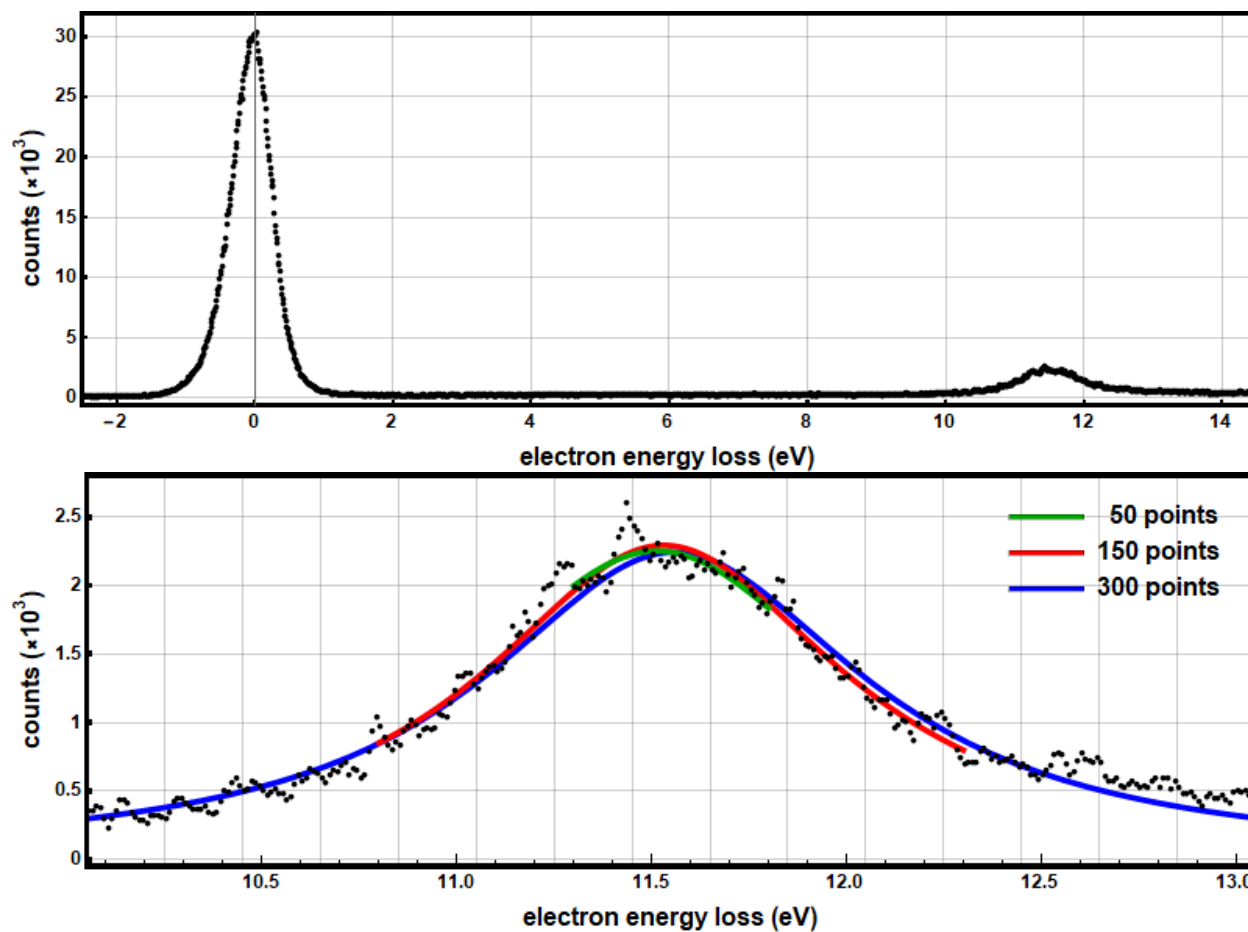
The energy of the indium plasmon described in the main text is defined to be the difference between the centers of the zero-loss peak (ZLP) and indium plasmon peak, as determined by fitting. We use a Gaussian and a Lorentzian function to fit the ZLP and indium plasmon peak, respectively. The fit windows for the Gaussian and Lorentzian fits are determined by a chi-squared (χ^2) test. Supporting Figure 8 shows the reduced χ^2 (blue) and the standard error (red) of the measured indium plasmon peak center *versus* the number of points included in the energy fit window for the data of Fig. 2 of the main text.

Plotting the reduced χ^2 statistic shows two distinct regions separated by an “elbow” (Supporting Figure 8, left). The overall shape of the curve indicates that the differences between the fit and the data are smaller (larger) for smaller (larger) fit windows. Past the “elbow” (*i.e.* the increase in slope) in the reduced- χ^2 -statistic plot, the fit function is no longer providing a good model of the data, and thus the fit parameters returned have no physical interpretation. We also plot (Supporting Figure 8, right), for the fit values returned for the peak center, the standard error-of-the-mean of the distribution supplied by the ~ 700 real-space pixels in the nanoparticle ROI (see PEET data analysis section). As the size of the fit window increases, the standard error decreases monotonically. Optimizing the fit window thus involves compromising between having a “good” fit and having “good” statistical precision. The width of the optimum fit window we take to be given by the position of the “elbow”, as that point broadens the energy window to the extent possible without unduly compromising the agreement between the fit function and the data. While it is difficult to locate the knee precisely, the full analysis is not sensitive to its exact location. Values in the range 110-170 might give slightly different values for the plasmon energy, but these changes amount to a constant offset: temperatures are determined by shifts in the plasmon energy, and that constant drops out in the difference between two plasmon energies.

Supporting Figure 9 shows the entire low-loss spectrum, and then fits to the indium plasmon that are based on small (50 point), optimal (150 point), and large (300 point) fit windows. Even though extreme values for the fit windows are shown, one value is not obviously preferred over the others. Thus the χ^2 analysis is required to objectively optimize the size of the fit window.



Supporting Figure 8: Examples of reduced χ^2 and standard error plots used for optimizing the plasmon fit window. The change in slope of the blue curve is the point at which the fit window is optimal: here we would chose a window with 150 fit points. (The plot of the standard error is truncated at 150 points because, while the calculated standard error continues to decrease smoothly, that number becomes less physically meaningful as the number of points continues to increase.)



Supporting Figure 9: (top) Single-pixel EELS spectrum from an indium nanoparticle. (bottom) Three Lorentzian fits to the indium plasmon, based on 50, 150, and 300 point fit windows. The spectrometer dispersion is 10 meV/point.

References

- (1) Mecklenburg, M.; Zutter, B.; Regan, B. C. Thermometry of Silicon Nanoparticles. *Phys. Rev. Appl.* **2018**, *9*, 014005.
- (2) Mecklenburg, M.; Hubbard, W. A.; White, E. R.; Dhall, R.; Cronin, S. B.; Aloni, S.; Regan, B. C. Nanoscale Temperature Mapping in Operating Microelectronic Devices. *Science* **2015**, *347*, 629–632.
- (3) Smith, J. F.; Schneider, V. L. Anisotropic Thermal Expansion of Indium. *J. Common Met.* **1964**, *7*, 17–22.